Supplemental Experimental Procedures

Cell line sources and validation

The cell lines Granta-519, Jeko-1, Mino, Rec-1, and Mec-1 were obtained from the Broad-Novartis Cancer cell line encyclopedia. Z-138, Maver-1, JVM-2, and HBL-2 cells were provided by Dr. Randy Gascoyne (BC Cancer Agency). SP-49 was the gift of Dr. Mariusz Wasik (University of Pennsylvania). Cell lines were verified as unique by short tandem repeat (STR) profiling and matched known STR profiles or, in lines for which profiles were not available (SP-49, HBL-2), matched published coding sequence polymorphisms (**Table S1**). Novel STR profiles for SP-49 and HBL-2 as well as loci and oligonucleotides used for genotyping are available upon request.

Human lymphoma biopsy selection and evaluation

CLL and MCL lymph node biopsies were genotyped for *NOTCH1* mutations and evaluated for high and low NICD1 expression by immunohistochemistry as described (Kluk et al., 2013). All biopsies used for RNA-Seq and ChIP-Seq studies were diffusely involved, with CLL cells representing >90% of cells based on immunohistochemical staining for CD20.

Notch ligand stimulation and time-course assay

For time-course experiments involving Notch activation in Mino and Jeko-1 cells, samples were plated 48 h prior to harvest in wells containing immobilized recombinant Notch ligand (DLL1^{ext}-IgG, a kind gift of Dr. Irwin Bernstein) or were plated in wells containing control-IgG and transferred to DLL1^{ext}-IgG-containing wells at the appropriate time point prior to harvest.

RNA-seq

Strand-specific RNA-seq was performed on MCL cell lines (three replicates per experimental condition) and purified MCL cells from PDX mice; detailed protocols are available on request. In brief, RNA was isolated from cell pellets with Qiashredder and RNEasy columns (Qiagen). Library preparation was similar to published protocols (Engreitz et al., 2013; Shishkin et al., 2015). Total RNA (2μg per sample) was subjected to poly-A selection with the Dynabeads mRNA DIRECT kit (Life Technology). RNA fragmentation was carried out with RNA fragmentation buffer (Life Technologies, AM8740). DNA was digested

with Turbo DNAse enzyme (Life Technologies, AM2238), and RNA was dephosphorylated with FastAP enzyme (Fermentas, EF0651). After RNA isolation with Dynabeads MyOne Silane beads (Life Technologies, 10977-015), RNA adaptor ligation (15pMol of adaptor RiT-20, IDT DNA; see below for adaptor and primer sequences) was performed with T4 RNA Ligase 1 (New England Biolabs, M0437M) in the presence of RNAse inhibitor (Applied Biosciences, #100021540). Following RNA clean up with Silane beads, 15pMol of primer rTd (IDT DNA) was annealed and first strand cDNA synthesis was performed with AffinityScript Reverse Transcriptase (Agilent, #600109). Primer cleanup was performed by adding ExoSap-it (Affymetrix, #78201) and RNA hydrolysis was performed with 100mM NaOH followed by neutralization with 100mM HCl. ssDNA was isolated with Silane beads and adaptor ligation, (100pMol of 5iLL-22 DNA adaptor, IDT DNA) was carried out with T4 RNA Ligase 1. Each ssDNA was then amplified by PCR with Phusion High-Fidelity PCR Master Mix (New England Biolabs, #M0531L) and 2P_univ and 2P_barcode primers (500nM each final concentration) and purified twice with Ampure XP beads (Beckman Coulter, A63881). Indexed libraries were validated for quality and size distribution using the Agilent 2100 Bioanalyzer and were sequenced on the HiSeq 2500 Illumina Genome Analyzer.

RNA-Seq library prep oligonucleotides:

Name	**Oligo type**	**Sequence**
RiT-19	RNA	/5Phos/rArGrArUrCrGrGrArArGrArGrCrArCrArCrGrUrC/3ddC
rTd RT	DNA	AGA CGT GTG CTC TTC CG
5ILL-22	DNA	/5Phos/AG ATC GGA AGA GCG TCG TGT AG/3ddC/
2P_universal	DNA	AATGATACGGCGACCACCGAGATCTACACTCTTTCC CTACACGACGCTCTTCCGATCT
2P_barcode	DNA	CAAGCAGAAGACGGCATACGAGATXXXXXXXXGTGACTGGAGTTCAGACGTGT GCTCTTCCGATCT

RNA-seq analysis of CLL lymph node biopsies was performed at the Center for Cancer Computational Biology at Dana Farber Cancer Institute (Boston, MA). Trizol was used for RNA isolation from frozen sections of lymph nodes involved by CLL. Using the Next Ultra RNA Library Prep Kit for Illumina (NEB), 100ng of total RNA was converted into a DNA library that was quantified using the Qubit High Sensitivity DNA Kit (Life Tech) and sized using the Bioanalyzer High Sensitivity Chip Kit (Agilent). Libraries were put through qPCR using the Universal Library Quantification Kit for Illumina (Kapa Biosystems) and run on the 7900HT Fast qPCR machine (ABI). Libraries passing quality control were sequenced on

the HiSeq 2000 (Illumina) at a final concentration of 12pM. Paired-end sequencing was performed with a total of 107 sequencing cycles per standard Illumina protocols.

Chromatin immunoprecipitation assay

ChIP-qPCR and ChIP-seq were performed as described (Ryan et al., 2015). Briefly, chromatin samples prepared from fixed cells were immunoprecipitated with antibodies recognizing NICD1 (Val1744 epitope, CST; #4147), RBPJ (CST, #5313), H3K27ac (Active Motif, #39133), EBNA2 (Abcam, ab90543), and MAML1 (CST; #12166), or with control rabbit IgG (Santa Cruz Biotechnology, sc-3888). Antibody-chromatin complexes were captured with protein G–conjugated beads, washed, and eluted. After reversal of cross-linking, RNase and proteinase K treatment were performed and DNA was purified and quantified for qPCR or library preparation. Input sample was prepared by the same approach without immunoprecipitation. For ChIP-PCR, real-time PCR was performed in triplicate for indicated regions using primers listed below. For ChIP-seq, libraries were prepared using NEBNext® Ultra™ DNA Library Prep Kit or as described (Ryan et al., 2015). Replicates were used for each experimental condition in GSI-washout or mock-washout H3K27ac (Rec-1, two replicates; SP-49, three replicates) and for NICD1 and RBPJ studies in Rec-1 (two replicates). Two replicates each were generated for Mino H3K27ac ChIP-Seq in the following experimental conditions: control IgG + DMSO; DLL1extIgG + DMSO; DLL1extIgG + GSI (4 h GSI-washout); and DLL1extIgG + GSI (4 h mock-washout). Indexed libraries were validated for quality and size distribution using an Agilent 2100 Bioanalyzer. Paired-end high-throughput sequencing (38 bp + 38 bp) was performed using the HiSeq 2500 Illumina Genome Analyzer.

Oligonucleotides used for quantitative ChIP-PCR

Locus	Forward	Reverse
5' MYC E1	CCCCCATGAAATCCCCATTGAAA	CCCTTATTTCCTCCAGTGCCTTTG
5' MYC E2	GAAGGCCTCCACCTGAGAAAGAG	CCAATACCTCTGGCTGTCCGC

4C-Seq

High-resolution 4C-Seq was performed as described (van de Werken et al., 2012a). Briefly, cells were crosslinked with 2% formaldehyde in PBS at room temperature for 10 minutes, followed by glycine quenching, washing in PBS, isolation of nuclei by hypotonic buffer lysis, and resuspension in primary restriction enzyme buffer. Primary digestion was

accomplished by sequential addition of SDS, Triton-X100, and primary restriction enzyme while mixing at 37°C, followed by heat inactivation at 65°C. Ligation was performed after sample dilution in T4 ligase buffer by addition of T4 ligase at 16°C. Ligated DNA was isolated by proteinase K and RNAase A digestion, phenol-chloroform extraction, and ethanol precipitation. DNA was then digested with secondary restriction enzyme, heat inactivated, ligated with T4 ligase, and isolated by ethanol precipitation and QIAquick PCR purification columns. To generate each 4C-Seq library, a total of 3.2 micrograms of 4C DNA was amplified across 16 separate 50-microliter PCR reactions containing Q5 high-fidelity polymerase mix (NEB) and oligonucleotides pairs consisting of universal illumina adaptor sequences, sample-specific barcodes, and viewpoint-specific primer sequences. Equal portions of each reaction were pooled and the PCR-amplified library was purified with 0.8 volumes of Ampure XP per volume of PCR product.

We selected 4-cutter restriction enzymes NlaIII (primary) and DpnII (secondary), for which high-quality viewpoint primers were available within 3 kB of the B-NDME E1 and E2 sites, as well as the MYC TSS in a pre-calculated hg19 4C-Seq primer database (primer_db, available at http://compgenomics.weizmann.ac.il/tanay/)

Oigonucleotide primers used for 4C-seq library generation. 'N' bases mark position of 8-mer multiplexing barcode in the non-view primer.

Locus	**View primer**	**Non-view primer**
5' MYC E1	AATGATACGGCGACCACCGAGATCTACAC TCTTTCCCTACACGACGCTCTTCCGATCT AAAGAATGAGTGTGGCCATG	CAAGCAGAAGACGGCATACGAGATNNNNNNNNG TGACTGGAGTTCAGACGTGTGCTCTTCCGATCT AGTTCAGGTATGCAAAGTGG
5' MYC E2	AATGATACGGCGACCACCGAGATCTACAC TCTTTCCCTACACGACGCTCTTCCGATCT GAAGTAATAATGCCTGCATG	CAAGCAGAAGACGGCATACGAGATNNNNNNNNG TGACTGGAGTTCAGACGTGTGCTCTTCCGATCT TATGTAAGGAACCACACAGAGA
MYC promoter	AATGATACGGCGACCACCGAGATCTACAC TCTTTCCCTACACGACGCTCTTCCGATCT AGCTGCTGGGAGGAGACATG	CAAGCAGAAGACGGCATACGAGATNNNNNNNNG TGACTGGAGTTCAGACGTGTGCTCTTCCGATCT CCACGTCCTAACACCTCTAG

4C-Seq data analysis used in Figure 2H was performed with 4CSeq-Pipe (van de Werken et al., 2012b) and analysis used for figure S2D was performed with FourCSeq (Klein et al., 2015) per the authors' instructions.

Lentiviral infection and cell sorting

Lentivirus was produced in HEK293T cells, harvested 48 h post-transfection, and subjected to 0.45 μm filtration. Cell lines were transduced with lentiviral supernatants by spinfection at 1000 x g for 90 min in the presence of 6μg/ml of polybrene at 37°C. For stable line generation, transduced populations were isolated by sorting on a BD FACSAria II SORP (pHR-SFFV-KRAB-dCas9-P2A-mCherry (Gilbert et al., 2014), pLX-304-GFP, pINDUCER-22 (Meerbrey et al., 2011)), or selected with 1mg/ml G418 (pINDUCER-20) for 10 d.

dCas9-KRAB analysis of *MYC* and *CR2* regulatory elements

GuideRNAs targeting sequences in the *MYC* and *CR2* loci (sequences provided below) were designed with the Broad Gene Perturbation Platform sgRNA designer (http://portals.broadinstitute.org/gpp/public/analysis-tools/sgrna-design) and cloned into lentiGuide-Puro (Addgene #52963). To study effects on *MYC* transcript levels, SFFV-KRAB-dCas9-P2A-mCherry+ cells were transduced in 96-well plates with gRNA lentivirus and grown for 3 d post-transduction. Cells were harvested and RNA extracted with the RNAdvance Cell v2 kit (Agencourt) per the manufacturer's instructions, followed by qRT-PCR quantification. To evaluate growth effects of *MYC* locus-specific gRNAs, a 1:1 mixture of pLX-304-GFP+ or SFFV-KRAB-dCas9-P2A-mCherry+ cells were infected with gRNA lentivirus in 96-well plates, selected with 1ng/mL puromycin after d 3, and harvested on d 7 for relative quantification of GFP+ and mCherry+ cells on a Cytoflex S flow cytometer (Beckman-Coulter). This latter protocol was also used to evaluate the effects of *CR2* locus gRNAs on CD21 surface protein expression in SP-49 and Granta-519, except that cells were stained with APC-anti-CD21 after harvest (clone HB5, Miltenyi) to determine relative expression levels on GFP+ and mCherry+ cells.

sgRNA target sequences:

GuideID	Gene / locus	Location	sgRNA target sequence	chr	start	end	strand
g015	GFP	Non-targeting control	GAGCTGGACGGCGACGTAAA	na	na	na	na
g004	MYC	BNDME-E1	TTTGCATTCTGAACCTAGCT	chr8	128222151	128222171	+
g005	MYC	BNDME-E1	GAAATCTGATATCTGTGGGA	chr8	128222409	128222429	-
g006	MYC	BNDME-E1	TATAGTAAACTCTTCAAAAG	chr8	128223027	128223047	-
g008	MYC	BNDME-E2	AAGGCCTCCACCTGAGAAAG	chr8	128315158	128315178	+
g009	MYC	BNDME-E2	GAGCACACTCTGTGAGAAAA	chr8	128315228	128315248	+
g010	MYC	BNDME-E2	CAGATGGCGGCTGGGTGGGA	chr8	128315370	128315390	-
g011	MYC	BNDME-E2	GCTTAGTCCATTTTACAGAT	chr8	128314888	128314908	+
g012	MYC	MYC promoter	TGCGAGGGTCTGGACGGCTG	chr8	128748292	128748312	+
g013	MYC	MYC promoter	CCCCCGAGCTGTGCTGCTCG	chr8	128748316	128748336	+

g014	MYC	MYC promoter	CCGCGAGCAGCACAGCTCGG	chr8	128748319	128748339	–
g080	MYC	MYC intergenic control	TAAGCTACAATAACATAGTG	chr8	128502378	128502398	+
g081	MYC	MYC intergenic control	ATAACACAATCAGGTCACAG	chr8	128603069	128603089	–
g095	MYC	TNDME	AGAAAGTTGATGAACCACAT	chr8	130180595	130180615	+
g099	MYC	TNDME	AGGCAGCTGGGAAATTATAT	chr8	130180292	130180312	+
g020	CR2	CR2 enhancer	GTTCTCATGAAGTCAAACGA	chr1	207603559	207603579	+
g021	CR2	CR2 enhancer	CACCAGTGCAACCTGCCATG	chr1	207603327	207603347	+
g022	CR2	CR2 enhancer	AGCACTGAGATAGAGCCACA	chr1	207603345	207603365	–
g023	CR2	CR2 enhancer	CCTTGGTTCCTATTTCCTAT	chr1	207605018	207605038	+
g024	CR2	CR2 enhancer	ATTCTCACAACAGTTCCCAT	chr1	207605036	207605056	–
g093	CR2	CR2 enhancer	GATTCAGTAGTTCCCAGGTG	chr1	207604099	207604119	+
g094	CR2	CR2 enhancer	AACCTGATTCAGTAGTTCCC	chr1	207604094	207604114	+
g026	CR2	CR2 promoter	GCAGCAAGCAGCTGTGAGCC	chr1	207627665	207627685	–
g101	CR2	CR2 intergenic control	TTATAACTTTATCAGATGCA	chr1	207609719	207609739	–

Oligonucleotides used for quantitative RT-PCR:

Gene	**Forward**	**Reverse**
MYC	ACCCTCTCAACGACAGCAGC	ACTCCGTCGAGGAGAGCAGA
CCND1	AGCTCCTGTGCTGCGAAGTG	GATCTTCCGCATGGACGGCA
EEF1A1	TTGTCGTCATTGGACACGTAG	TGCCACCGCATTTATAGATCAG

Immunohistochemistry

Paraffin-embedded tissue sections (4-micron) were stained on the Ventana Benchmark XT platform (Ventana Medical Systems, Inc., Tucson, AZ.) with extended heat-induced epitope retrieval (CC1 Buffer). Slides were incubated for 1 h at room temperature with anti-NICD1 rabbit monoclonal antibody (clone D3B8, catalog #4147, Cell Signaling Technology, Beverly, MA; final concentration, 8.5µg/mL) or rabbit monoclonal anti-human MYC (catalog # 1472-1, Epitomics, Inc., Burlingame, CA, USA final concentration 0.56mg/ml). Signal amplification (Ventana Amplification Kit, #760-080) and visualization (Ventana Ultraview Universal DAB detection kit, #760-500) were performed per the manufacturer's instructions. Staining results were scored by two hematopathologists (NICD1: JCA and MK; MYC: JCA and RR).

Patient-derived xenograft (PDX) GSI treatment experiments

PDX DFBL-98848 was established through the Public Repository of Xenografts (PRoXe) program, with complete methods and protocols, as well as xenograft distribution information available at http://www.proxe.org. For pharmacodynamic experiments with the GSI DBZ, DFBL-98848 xenografts were established in 10 female 6 week-old NOD-*scid*-

gamma mice via tail vein injection of $1.5x10^6$ cells. Treatment was initiated upon appearance of MCL cells in the peripheral blood at d 32 and consisted of IP injection of DBZ (10μMol/kg) in 0.5% CMC + 1% Tween 80 or vehicle alone every other day for 5 d. One mouse in the DBZ treatment group died on d 4 (36 d after cell injection) and was excluded from further analysis. Mice were sacrificed following the final treatment. Cells were isolated from spleen by mechanical disaggregation and red blood cell lysis, and from bone marrow by flushing of femurs and tibias with saline. Subsequent cell processing steps for all samples were performed on ice and in the presence of 1 μM Compound E to prevent *ex vivo* activation of Notch. Human cells were isolated from mouse spleen cells by EasySep Mouse/Human Chimera Isolation Kit (STEMCELL Technologies) per the manufacturer's protocol and flash-frozen for RNA-Seq analysis. Notch target gene expression was assessed on human $CD19^+CD5^+$ cells from spleen, bone marrow, and peripheral blood with the following panel: CD19-APC (HIB19, Biolegend), CD5 PE-Cy7 (L17F12, BioLegend), CD300A-PE (Beckman-Coulter), and SEMA7A-FITC (Abcam).

MYC and *CCND1* rearrangement detection

Interphase FISH was performed with the Vysis LSI *MYC* Dual Color Break Apart Rearrangement Probe and the Vysis LSI *IGH*/*MYC*/CEP8 Tricolor Dual Fusion Translocation Probe (Abbott Molecular). Results with the *MYC* break-apart probe in Rec-1, Jeko-1, Granta-549, and Mino cells were reported previously (Ryan et al., 2015). Because the results of dual fusion *IGH*/*MYC* FISH showed clear evidence of a *MYC*-*IGH* rearrangement in Mino, we repeated break-apart studies in this line and noted two non-split signals, as well as a faint single red signal that had not been observed in the prior study, consistent with the presence of an unbalanced *MYC* rearrangement. PEAR-ChIP analysis for localization of rearrangement breakpoints (Ryan et al., 2015) was performed on H3K27ac ChIP-Seq data from all cell lines and included manual review of all rearranged *MYC* and *CCND1* sequences.

RNA-Seq data analysis

For MCL cell lines and PDX experiments, RNA-Seq reads were aligned to hg19 using TopHat2. Rec-1, CUTLL1, and HCC-1599 data (Stoeck et al., 2014) were reprocessed with the same methodology. HTSeq was used to quantify reads mapping to the iGenomes UCSC genes hg19 transcript annotation, with read-through genes removed to prevent exon exclusion. Differential gene expression analysis was performed with DESeq2 (Love et al.,

2014), using default settings. In cell line experiments, genes were considered differentially expressed that showed log2 fold change > 0.2 or < -0.2 and FDR-adjusted p-value <0.05. Genes meeting criteria for increased expression in the GSI-washout (Notch-on) versus mock-washout state in at least 2 MCL lines were assigned to Group 1 (1a, 1b, 1c) or Group 2 as described in the text and figures. Genes with concordantly decreased expression in the Notch-on state in two or more lines were assigned to Group1-down (1a-down, 1b-down, 1c-down) or Group2-down by the same schema.

For primary CLL samples, RNA-Seq reads were aligned to hg19 with STAR and differential analysis was performed with DESeq2 using local fit for dispersion calculation. To visualize the relative gene expression level for CLL samples, we applied a regularized log transformation to the counts of each gene using rlog from DESeq2 and calculated the median-centered z-score across the samples. We used Fisher's exact test (one-tailed) to determine the significance and odds ratio for over-representation of MCL-defined Notch target gene sets among genes up-regulated in *NOTCH1*-mutant CLL or down-regulated in DBZ-treated PDX mice with nominal p-value < 0.05. Gene set enrichment analysis was performed with the GSEA Java desktop application using the GSEA pre-ranked function, ranking of genes based on log2fold change for the indicated experimental contrasts (based on DESeq2 analysis), and gene sets from the mSigDB Hallmark and Reactome collections or custom Notch target gene sets defined in this study. GSEA display plots were generated with ReplotGSEA.R (https://github.com/PeeperLab/Rtoolbox/blob/master/R/ReplotGSEA.R,). The direct Notch target signature (B-NOTCH-DIRECT) is listed in Table S4 / Tab-1. The signature FABBRI-CLL-NOTCH was obtained from (Fabbri et al., 2017) - Supplementary dataset S9. The signature B-NOTCH-DIRECT_UNIQUE consists of genes present in B-NOTCH-DIRECT but not FABBRI-CLL-NOTCH. Ingenuity Canonical Pathways analysis was performed with the Group 1 Notch target genes using recommended default parameters.

To compare transcript abundance of candidate Notch target genes on a transcript length-independent scale (transcripts per million; TPM), RNA-Seq fastq files were pseudo-aligned to the iGenomes UCSC genes hg19 transcript annotation with Kallisto (Bray et al., 2016), and then abundance was summarized at the gene level with tximport (Soneson et al., 2015).

ChIP-Seq data analysis

ChIP-Seq reads were aligned to hg19 using BWA-ALN and filtered to remove PCR duplicates and reads mapping to >2 sites genome-wide. ChIP-Seq display files were generated with "igvtools count" and visualized with IGV. Scaling for all ChIP-Seq tracks in figures is equal to local paired-end fragment coverage x (1,000,000 / totalCount). Unless otherwise specified, H3K27ac tracks shown in figures as "MCL LN biopsy" and "CLL LN biopsy" correspond to datasets generated from samples MCL-03 and SLL-03, respectively (Ryan et al., 2015). Transcription factor ChIP-Seq peak calling was performed with HOMER findPeaks using the "factor" style and default settings (FDR threshold 0.001, with significant peaks post-filtered for 4-fold enrichment over local and input tag counts) for cell line datasets. Identical settings were used for CLL lymph node ChIP-Seq datasets except that post-filtering was set at 3-fold enrichment to reduce filtering of significant but low-amplitude peaks. All peak sets were also post-filtered for known ENCODE blacklist regions (available at http://hgdownload.cse.ucsc.edu/goldenpath/hg19/encodeDCC/wgEncodeMapability/wgEncodeDacMapabilityConsensusExcludable.bed.gz). Replicate ChIP-Seq datasets for Rec-1 NICD1 (GSI-washout) and Rec-1 RBPJ (GSI-washout) were analyzed with the Irreproducibility Discovery Rate framework, and met ENCODE criteria for peak reproducibility (Landt et al., 2012). The corresponding mock-washout datasets showed few peaks as expected. We therefore merged replicate datasets and used the merged datasets for all further analysis and figures except where indicated. *De novo* DNA motif enrichment analysis was performed with HOMER findMotifs and known motif analysis was performed with the HOMER motif library version 4.6.

To generate the set of consensus NTC peaks we compared NTC peaks in the Notch-on state within each MCL cell line (Rec-1: NICD1 (GSI-washout)-merged, RBPJ, MAML1; SP-49 RBPJ, MAML1; Mino(Dll1extIgG): NICD1, RBPJ). Homer mergePeaks (-prefix -d 200) was used to identify reproducible peaks (centers within 200 bp) for at least two proteins in the same cell line. The union of such peaks across all Rec-1, SP-49, and Mino cells were included in the consensus NTC binding sites. We also observed that a small number of strongly Notch-activated genes (e.g. *NOTCH3*) were associated with sites that showed reproducible, GSI-sensitive NICD1 binding, but minimal binding of other NTC proteins, so we also included sites bound in three independent Notch-on NICD1 ChIP-Seq datasets (Rec-1: NICD1 (gsi-washout) replicates 1 and 2, and Mino(Dll1extIgG) NICD1).

For differential H3K27ac analysis, peak calling was performed using MAC2 (version 2.0.9), with the following parameters: --nomodel, --shiftsize=(1/2 estimated fragment length), --keep-dup=1 and FDR threshold 1E-6. Regions of 1kb flanking the summits of peaks identified in the washout condition were merged across replicates using bedtools-merge (version 2.25.0), generating a total of 72,576 H3K27ac enriched regions. In each library, peak-filtered H3K27ac signal was quantified and normalized to fragment per kilo-base per million reads (FPKM) and the H3K27ac regions with median read counts of <50 across all libraries were removed. The remaining H3K27ac-enriched regions were annotated as NTC-bound or -unbound based on the overlap with consensus NTC peaks using bedtools-intersect. HOMER-annotatePeaks (version 4.8) was used to annotate H3K27ac regions. Regions >5 kb from TSSs were denoted as distal. For each cell line, the logarithmic fold change of H3K27ac load on distal H3K27ac regions with non-zero read counts in at least one library was calculated as log2 FPKM of the mean of washout replicates versus the mean of GSI replicates with a pseudo-count of 1. The log2 fold change of NTC bound/unbound distal reference regions in each cell line was visualized with geom_boxplot from ggplot2 package in R (version 3.2.3), with the whiskers limited to 1.5*IQR. R function t test was used for statistical comparison of NTC bound/unbound log2 fold change.

NTC peak / gene linkage analysis

Expressed genes in each cell line were defined as genes passing default independent filtering threshold in DESeq2. For each expressed gene, TSS-proximal regions were defined as all annotated transcriptional start sites +/- 5 kb. Linkage between an individual NTC consensus binding site (flanked by 500 bp) and an expressed gene was defined as: 1) 'Proximal' when a flanked NTC region overlapped a TSS-proximal region for that gene; 2) 'Distal' when condition 1 did not apply, but the flanking NTC binding site was linked to a TSS-proximal region for that gene by RNA-Pol2 ChIA-PET clusters in GM12878 cell line (GEO accession number: GSM1872887); 3) 'CCD' (chromatin contact domain) when conditions 1 and 2 did not apply, but the flanking NTC binding site fell within the same CTCF-mediated chromatin contact domain (defined in the GM12878 cell line, see GSM1872886) as a TSS-proximal region for the gene. Each gene could then be classified into one of five mutually exclusive categories, depending on whether the gene demonstrated a) one or more proximal linkages (but not distal), b) one or more distal linkages (but not proximal), c) both proximal and distal linkages, d) one or more CCD linkages (but not

proximal or distal), e) no linkages. *MYC* and Group 1 genes in categories a), b), or c) were classified as direct NTC-linked Notch target genes.

Permutation testing was used to demonstrate the significance of the proportion of Group 1 genes linked to NTC binding sites. A Gaussian bimodal kernel estimation was applied to the mean FPKM of the expressed genes across all the washout samples to defined the low and high expressed genes. The control gene set is defined as expressed genes that are not Notch-sensitive. The Null distribution for gene / NTC binding site linkage was generated by iterative sampling (n = 10,000) of the control genes with cardinality equal to set G1 while controlling for the ratio of the high/low expression. For the purpose of cross-tissue comparisons of gene expression, high-confidence direct Notch target genes identified in MCL were considered to be activated in CUTLL1 or HCC-1599 if they showed a log2 fold change > 0.2, regardless of significance. For visualization, DNA Landscaper (http://dnalandscaper.aryeelab.org/) was used to plot GM12878 Pol2 ChIA-PET loops over selected genomic intervals.

Summary of datasets

Dataset number	Dataset title	Dataset type	Original study	GEO accession	dbGaP accession
Dataset 1	HBL2_H3K27ac	ChIP-Seq	This study	GSE97541	Not applicable
Dataset 2	HBL2_wce	ChIP-Seq	This study	GSE97541	Not applicable
Dataset 3	JVM2_H3K27ac	ChIP-Seq	This study	GSE97541	Not applicable
Dataset 4	JVM2_wce	ChIP-Seq	This study	GSE97541	Not applicable
Dataset 5	Maver-1_H3K27ac	ChIP-Seq	This study	GSE97541	Not applicable
Dataset 6	Maver-1_wce	ChIP-Seq	This study	GSE97541	Not applicable
Dataset 7	Mino_ctrl-IgG-DMSO_H3K27ac_r1	ChIP-Seq	This study	GSE97541	Not applicable
Dataset 8	Mino_ctrl-IgG-DMSO_H3K27ac_r2	ChIP-Seq	This study	GSE97541	Not applicable
Dataset 9	Mino_DLL1-IgG-DMSO_H3K27ac_r1	ChIP-Seq	This study	GSE97541	Not applicable
Dataset 10	Mino_DLL1-IgG-DMSO_H3K27ac_r2	ChIP-Seq	This study	GSE97541	Not applicable
Dataset 11	Mino_DLL1-IgG-DMSO_NICD1	ChIP-Seq	This study	GSE97541	Not applicable
Dataset 12	Mino_DLL1-IgG-DMSO_RBPJ	ChIP-Seq	This study	GSE97541	Not applicable
Dataset 13	Mino_DLL1-IgG-gsi-gsi_H3K27ac_r1	ChIP-Seq	This study	GSE97541	Not applicable
Dataset 14	Mino_DLL1-IgG-gsi-gsi_H3K27ac_r2	ChIP-Seq	This study	GSE97541	Not applicable
Dataset 15	Mino_DLL1-IgG-gsi-wo_H3K27ac_r1	ChIP-Seq	This study	GSE97541	Not applicable
Dataset 16	Mino_DLL1-IgG-gsi-wo_H3K27ac_r2	ChIP-Seq	This study	GSE97541	Not applicable
Dataset 17	Rec-1_H3K27ac_gsi-gsi-r1	ChIP-Seq	This study	GSE97541	Not applicable
Dataset 18	Rec-1_H3K27ac_gsi-gsi-r2	ChIP-Seq	This study	GSE97541	Not applicable
Dataset 19	Rec-1_H3K27ac_gsi-wo-r1	ChIP-Seq	This study	GSE97541	Not applicable
Dataset 20	Rec-1_H3K27ac_gsi-wo-r2	ChIP-Seq	This study	GSE97541	Not applicable
Dataset 21	Rec-1_MAML1	ChIP-Seq	This study	GSE97541	Not applicable

Dataset 22	Rec-1_NICD1_gsi-gsi-r1	ChIP-Seq	This study	GSE97541	Not applicable
Dataset 23	Rec-1_NICD1_gsi-gsi-r2	ChIP-Seq	This study	GSE97541	Not applicable
Dataset 24	Rec-1_NICD1_gsi-wo-r1	ChIP-Seq	This study	GSE97541	Not applicable
Dataset 25	Rec-1_NICD1_gsi-wo-r2	ChIP-Seq	This study	GSE97541	Not applicable
Dataset 26	Rec-1_RBPJ	ChIP-Seq	This study	GSE97541	Not applicable
Dataset 27	Rec-1_RBPJ_gsi-gsi-r1	ChIP-Seq	This study	GSE97541	Not applicable
Dataset 28	Rec-1_RBPJ_gsi-gsi-r2	ChIP-Seq	This study	GSE97541	Not applicable
Dataset 29	Rec-1_RBPJ_gsi-wo-r1	ChIP-Seq	This study	GSE97541	Not applicable
Dataset 30	Rec-1_RBPJ_gsi-wo-r2	ChIP-Seq	This study	GSE97541	Not applicable
Dataset 31	SP-49_dmso_H3K27ac-r1	ChIP-Seq	This study	GSE97541	Not applicable
Dataset 32	SP-49_dmso_H3K27ac-r2	ChIP-Seq	This study	GSE97541	Not applicable
Dataset 33	SP-49_dmso_H3K27ac-r3	ChIP-Seq	This study	GSE97541	Not applicable
Dataset 34	SP-49_gsi-gsi_H3K27ac-r1	ChIP-Seq	This study	GSE97541	Not applicable
Dataset 35	SP-49_gsi-gsi_H3K27ac-r2	ChIP-Seq	This study	GSE97541	Not applicable
Dataset 36	SP-49_gsi-gsi_H3K27ac-r3	ChIP-Seq	This study	GSE97541	Not applicable
Dataset 37	SP-49_gsi-wo_H3K27ac-r1	ChIP-Seq	This study	GSE97541	Not applicable
Dataset 38	SP-49_gsi-wo_H3K27ac-r2	ChIP-Seq	This study	GSE97541	Not applicable
Dataset 39	SP-49_gsi-wo_H3K27ac-r3	ChIP-Seq	This study	GSE97541	Not applicable
Dataset 40	SP-49_H3K27ac	ChIP-Seq	This study	GSE97541	Not applicable
Dataset 41	SP-49_MAML1	ChIP-Seq	This study	GSE97541	Not applicable
Dataset 42	SP-49_RBPJ	ChIP-Seq	This study	GSE97541	Not applicable
Dataset 43	SP-49_wce	ChIP-Seq	This study	GSE97541	Not applicable
Dataset 44	Z138_H3K27ac	ChIP-Seq	This study	GSE97541	Not applicable
Dataset 45	Z138_wce	ChIP-Seq	This study	GSE97541	Not applicable
Dataset 46	Mec-1_H3K27ac	ChIP-Seq	This study	GSE97541	Not applicable
Dataset 47	Mec-1_wce	ChIP-Seq	This study	GSE97541	Not applicable
Dataset 48	Mino_ctrl-IgG-DMSO_RNA-Seq_r1	RNA-Seq	This study	GSE97541	Not applicable
Dataset 49	Mino_ctrl-IgG-DMSO_RNA-Seq_r2	RNA-Seq	This study	GSE97541	Not applicable
Dataset 50	Mino_ctrl-IgG-DMSO_RNA-Seq_r3	RNA-Seq	This study	GSE97541	Not applicable
Dataset 51	Mino_DLL1-IgG-DMSO_RNA-Seq_r1	RNA-Seq	This study	GSE97541	Not applicable
Dataset 52	Mino_DLL1-IgG-DMSO_RNA-Seq_r2	RNA-Seq	This study	GSE97541	Not applicable
Dataset 53	Mino_DLL1-IgG-DMSO_RNA-Seq_r3	RNA-Seq	This study	GSE97541	Not applicable
Dataset 54	Mino_DLL1-IgG-gsi-gsi_RNA-Seq_r1	RNA-Seq	This study	GSE97541	Not applicable
Dataset 55	Mino_DLL1-IgG-gsi-gsi_RNA-Seq_r2	RNA-Seq	This study	GSE97541	Not applicable
Dataset 56	Mino_DLL1-IgG-gsi-gsi_RNA-Seq_r3	RNA-Seq	This study	GSE97541	Not applicable
Dataset 57	Mino_DLL1-IgG-gsi-wo_RNA-Seq_r1	RNA-Seq	This study	GSE97541	Not applicable
Dataset 58	Mino_DLL1-IgG-gsi-wo_RNA-Seq_r2	RNA-Seq	This study	GSE97541	Not applicable
Dataset 59	Mino_DLL1-IgG-gsi-wo_RNA-Seq_r3	RNA-Seq	This study	GSE97541	Not applicable
Dataset 60	SP49_dmso_RNA-Seq_r1	RNA-Seq	This study	GSE97541	Not applicable
Dataset 61	SP49_dmso_RNA-Seq_r2	RNA-Seq	This study	GSE97541	Not applicable
Dataset 62	SP49_dmso_RNA-Seq_r3	RNA-Seq	This study	GSE97541	Not applicable
Dataset 63	SP49_gsi-gsi_RNA-Seq_r1	RNA-Seq	This study	GSE97541	Not applicable
Dataset 64	SP49_gsi-gsi_RNA-Seq_r2	RNA-Seq	This study	GSE97541	Not applicable
Dataset 65	SP49_gsi-gsi_RNA-Seq_r3	RNA-Seq	This study	GSE97541	Not applicable
Dataset 66	SP49_gsi-wo_RNA-Seq_r1	RNA-Seq	This study	GSE97541	Not applicable
Dataset 67	SP49_gsi-wo_RNA-Seq_r2	RNA-Seq	This study	GSE97541	Not applicable
Dataset 68	SP49_gsi-wo_RNA-Seq_r3	RNA-Seq	This study	GSE97541	Not applicable

Dataset 69	Rec1-DMSO-rep1-4C-BNDME1	4C-Seq	This study	GSE97541	Not applicable
Dataset 70	Rec1-DMSO-rep2-4C-BNDME1	4C-Seq	This study	GSE97541	Not applicable
Dataset 71	Rec1-GSI-rep1-4C-BNDME1	4C-Seq	This study	GSE97541	Not applicable
Dataset 72	Rec1-GSI-rep2-4C-BNDME1	4C-Seq	This study	GSE97541	Not applicable
Dataset 73	Rec1-DMSO-rep1-4C-BNDME2	4C-Seq	This study	GSE97541	Not applicable
Dataset 74	Rec1-DMSO-rep2-4C-BNDME2	4C-Seq	This study	GSE97541	Not applicable
Dataset 75	Rec1-GSI-rep1-4C-BNDME2	4C-Seq	This study	GSE97541	Not applicable
Dataset 76	Rec1-GSI-rep2-4C-BNDME2	4C-Seq	This study	GSE97541	Not applicable
Dataset 77	Rec1-DMSO-rep1-4C-MYCP	4C-Seq	This study	GSE97541	Not applicable
Dataset 78	Rec1-DMSO-rep2-4C-MYCP	4C-Seq	This study	GSE97541	Not applicable
Dataset 79	Rec1-GSI-rep1-4C-MYCP	4C-Seq	This study	GSE97541	Not applicable
Dataset 80	Rec1-GSI-rep2-4C-MYCP	4C-Seq	This study	GSE97541	Not applicable
Dataset 81	MCL-M06_H3K27ac	ChIP-Seq	This study	GSE97541	phs000939
Dataset 82	MCL-M06_wce	ChIP-Seq	This study	GSE97541	phs000939
Dataset 83	MCL-M08_H3K27ac	ChIP-Seq	This study	GSE97541	phs000939
Dataset 84	MCL-M08_wce	ChIP-Seq	This study	GSE97541	phs000939
Dataset 85	MCL-M10_H3K27ac	ChIP-Seq	This study	GSE97541	phs000939
Dataset 86	MCL-M10_wce	ChIP-Seq	This study	GSE97541	phs000939
Dataset 87	CLL-M10_H3K27ac	ChIP-Seq	This study	GSE97541	phs000939
Dataset 88	CLL-M10_wce	ChIP-Seq	This study	GSE97541	phs000939
Dataset 89	CLL-M12_H3K27ac	ChIP-Seq	This study	GSE97541	phs000939
Dataset 90	CLL-M12_wce	ChIP-Seq	This study	GSE97541	phs000939
Dataset 91	CLL-M13_H3K27ac	ChIP-Seq	This study	GSE97541	phs000939
Dataset 92	CLL-M13_NICD1	ChIP-Seq	This study	GSE97541	phs000939
Dataset 93	CLL-M13_RBPJ	ChIP-Seq	This study	GSE97541	phs000939
Dataset 94	CLL-M13_wce	ChIP-Seq	This study	GSE97541	phs000939
Dataset 95	PDX98848_1_RNA-Seq_veh	RNA-Seq	This study	GSE97541	Not applicable
Dataset 96	PDX98848_2_RNA-Seq_veh	RNA-Seq	This study	GSE97541	Not applicable
Dataset 97	PDX98848_3_RNA-Seq_veh	RNA-Seq	This study	GSE97541	Not applicable
Dataset 98	PDX98848_4_RNA-Seq_veh	RNA-Seq	This study	GSE97541	Not applicable
Dataset 99	PDX98848_5_RNA-Seq_veh	RNA-Seq	This study	GSE97541	Not applicable
Dataset 100	PDX98848_6_RNA-Seq_dbz	RNA-Seq	This study	GSE97541	Not applicable
Dataset 101	PDX98848_7_RNA-Seq_dbz	RNA-Seq	This study	GSE97541	Not applicable
Dataset 102	PDX98848_8_RNA-Seq_dbz	RNA-Seq	This study	GSE97541	Not applicable
Dataset 103	PDX98848_9_RNA-Seq_dbz	RNA-Seq	This study	GSE97541	Not applicable
Dataset 104	CLL-B01_RNA-Seq-Notch1WT-ICN1low	RNA-Seq	This study	GSE97541	Not applicable
Dataset 105	CLL-B02_RNA-Seq-Notch1WT-ICN1low	RNA-Seq	This study	GSE97541	Not applicable
Dataset 106	CLL-B03_RNA-Seq-Notch1WT-ICN1low	RNA-Seq	This study	GSE97541	Not applicable
Dataset 107	CLL-B04_RNA-Seq-Notch1WT-ICN1low	RNA-Seq	This study	GSE97541	Not applicable
Dataset 108	CLL-B05_RNA-Seq-Notch1Mut-ICN1high	RNA-Seq	This study	GSE97541	Not applicable
Dataset 109	CLL-B06_RNA-Seq-Notch1Mut-ICN1high	RNA-Seq	This study	GSE97541	Not applicable
Dataset 110	CLL-B07_RNA-Seq-Notch1Mut-ICN1high	RNA-Seq	This study	GSE97541	Not applicable
Dataset 111	CLL-B08_RNA-Seq-Notch1Mut-ICN1high	RNA-Seq	This study	GSE97541	Not applicable
Dataset 112	Granta-519_H3K27ac	ChIP-Seq	Ryan et al., Cancer Discovery 2016	GSE69558	Not applicable
Dataset 113	Rec-1_H3K27ac	ChIP-Seq	Ryan et al., Cancer Discovery 2016	GSE69558	Not applicable
Dataset 114	Mino_H3K27ac	ChIP-Seq	Ryan et al., Cancer Discovery 2016	GSE69558	Not applicable

Dataset 115	Jeko-1_H3K27ac	ChIP-Seq	Ryan et al., Cancer Discovery 2016	GSE69558	Not applicable
Dataset 116	Granta-519_wce	ChIP-Seq	Ryan et al., Cancer Discovery 2016	GSE69558	Not applicable
Dataset 117	Rec-1_wce	ChIP-Seq	Ryan et al., Cancer Discovery 2016	GSE69558	Not applicable
Dataset 118	Mino_wce	ChIP-Seq	Ryan et al., Cancer Discovery 2016	GSE69558	Not applicable
Dataset 119	Jeko-1_wce	ChIP-Seq	Ryan et al., Cancer Discovery 2016	GSE69558	Not applicable
Dataset 120	DLBCL-M02_H3K27ac	ChIP-Seq	Ryan et al., Cancer Discovery 2016	GSE69558	phs000939
Dataset 121	DLBCL-M02_wce	ChIP-Seq	Ryan et al., Cancer Discovery 2016	GSE69558	phs000939
Dataset 122	DLBCL-M03_H3K27ac	ChIP-Seq	Ryan et al., Cancer Discovery 2016	GSE69558	phs000939
Dataset 123	DLBCL-M03_wce	ChIP-Seq	Ryan et al., Cancer Discovery 2016	GSE69558	phs000939
Dataset 124	DLBCL-M04_H3K27ac	ChIP-Seq	Ryan et al., Cancer Discovery 2016	GSE69558	phs000939
Dataset 125	DLBCL-M04_wce	ChIP-Seq	Ryan et al., Cancer Discovery 2016	GSE69558	phs000939
Dataset 126	DLBCL-M05_H3K27ac	ChIP-Seq	Ryan et al., Cancer Discovery 2016	GSE69558	phs000939
Dataset 127	DLBCL-M05_wce	ChIP-Seq	Ryan et al., Cancer Discovery 2016	GSE69558	phs000939
Dataset 128	DLBCL-M07_H3K27ac	ChIP-Seq	Ryan et al., Cancer Discovery 2016	GSE69558	phs000939
Dataset 129	DLBCL-M07_wce	ChIP-Seq	Ryan et al., Cancer Discovery 2016	GSE69558	phs000939
Dataset 130	DLBCL-M10_H3K27ac	ChIP-Seq	Ryan et al., Cancer Discovery 2016	GSE69558	phs000939
Dataset 131	DLBCL-M10_wce	ChIP-Seq	Ryan et al., Cancer Discovery 2016	GSE69558	phs000939
Dataset 132	DLBCL-M11_H3K27ac	ChIP-Seq	Ryan et al., Cancer Discovery 2016	GSE69558	phs000939
Dataset 133	DLBCL-M11_wce	ChIP-Seq	Ryan et al., Cancer Discovery 2016	GSE69558	phs000939
Dataset 134	MCL-M01_H3K27ac	ChIP-Seq	Ryan et al., Cancer Discovery 2016	GSE69558	phs000939
Dataset 135	MCL-M01_wce	ChIP-Seq	Ryan et al., Cancer Discovery 2016	GSE69558	phs000939
Dataset 136	MCL-M02_H3K27ac	ChIP-Seq	Ryan et al., Cancer Discovery 2016	GSE69558	phs000939
Dataset 137	MCL-M02_wce	ChIP-Seq	Ryan et al., Cancer Discovery 2016	GSE69558	phs000939
Dataset 138	MCL-M03_H3K27ac	ChIP-Seq	Ryan et al., Cancer Discovery 2016	GSE69558	phs000939
Dataset 139	MCL-M03_wce	ChIP-Seq	Ryan et al., Cancer Discovery 2016	GSE69558	phs000939
Dataset 140	MCL-M04_H3K27ac	ChIP-Seq	Ryan et al., Cancer Discovery 2016	GSE69558	phs000939
Dataset 141	MCL-M04_wce	ChIP-Seq	Ryan et al., Cancer Discovery 2016	GSE69558	phs000939
Dataset 142	CLL-M02_H3K27ac	ChIP-Seq	Ryan et al., Cancer Discovery 2016	GSE69558	phs000939
Dataset 143	CLL-M02_wce	ChIP-Seq	Ryan et al., Cancer Discovery 2016	GSE69558	phs000939
Dataset 144	CLL-M05_H3K27ac	ChIP-Seq	Ryan et al., Cancer Discovery 2016	GSE69558	phs000939
Dataset 145	CLL-M05_wce	ChIP-Seq	Ryan et al., Cancer Discovery 2016	GSE69558	phs000939
Dataset 146	CLL-M07_H3K27ac	ChIP-Seq	Ryan et al., Cancer Discovery 2016	GSE69558	phs000939
Dataset 147	CLL-M07_wce	ChIP-Seq	Ryan et al., Cancer Discovery 2016	GSE69558	phs000939
Dataset 148	CUTLL1_control_1	RNA-Seq	Stoeck et al., Cancer Discovery 2014	GSE59810	Not applicable

Dataset 149	CUTLL1_control_2	RNA-Seq	Stoeck et al., Cancer Discovery 2014	GSE59810	Not applicable
Dataset 150	CUTLL1_control_3	RNA-Seq	Stoeck et al., Cancer Discovery 2014	GSE59810	Not applicable
Dataset 151	CUTLL1_gsi-gsi_1	RNA-Seq	Stoeck et al., Cancer Discovery 2014	GSE59810	Not applicable
Dataset 152	CUTLL1_gsi-gsi_2	RNA-Seq	Stoeck et al., Cancer Discovery 2014	GSE59810	Not applicable
Dataset 153	CUTLL1_gsi-gsi_3	RNA-Seq	Stoeck et al., Cancer Discovery 2014	GSE59810	Not applicable
Dataset 154	CUTLL1_gsi-wo_1	RNA-Seq	Stoeck et al., Cancer Discovery 2014	GSE59810	Not applicable
Dataset 155	CUTLL1_gsi-wo_2	RNA-Seq	Stoeck et al., Cancer Discovery 2014	GSE59810	Not applicable
Dataset 156	CUTLL1_gsi-wo_3	RNA-Seq	Stoeck et al., Cancer Discovery 2014	GSE59810	Not applicable
Dataset 157	HCC1599_control_1	RNA-Seq	Stoeck et al., Cancer Discovery 2014	GSE59810	Not applicable
Dataset 158	HCC1599_control_2	RNA-Seq	Stoeck et al., Cancer Discovery 2014	GSE59810	Not applicable
Dataset 159	HCC1599_control_3	RNA-Seq	Stoeck et al., Cancer Discovery 2014	GSE59810	Not applicable
Dataset 160	HCC1599_gsi-gsi_1	RNA-Seq	Stoeck et al., Cancer Discovery 2014	GSE59810	Not applicable
Dataset 161	HCC1599_gsi-gsi_2	RNA-Seq	Stoeck et al., Cancer Discovery 2014	GSE59810	Not applicable
Dataset 162	HCC1599_gsi-gsi_3	RNA-Seq	Stoeck et al., Cancer Discovery 2014	GSE59810	Not applicable
Dataset 163	HCC1599_gsi-wo_1	RNA-Seq	Stoeck et al., Cancer Discovery 2014	GSE59810	Not applicable
Dataset 164	HCC1599_gsi-wo_2	RNA-Seq	Stoeck et al., Cancer Discovery 2014	GSE59810	Not applicable
Dataset 165	HCC1599_gsi-wo_3	RNA-Seq	Stoeck et al., Cancer Discovery 2014	GSE59810	Not applicable
Dataset 166	REC1_control_1	RNA-Seq	Stoeck et al., Cancer Discovery 2014	GSE59810	Not applicable
Dataset 167	REC1_control_2	RNA-Seq	Stoeck et al., Cancer Discovery 2014	GSE59810	Not applicable
Dataset 168	REC1_control_3	RNA-Seq	Stoeck et al., Cancer Discovery 2014	GSE59810	Not applicable
Dataset 169	REC1_gsi-gsi_1	RNA-Seq	Stoeck et al., Cancer Discovery 2014	GSE59810	Not applicable
Dataset 170	REC1_gsi-gsi_2	RNA-Seq	Stoeck et al., Cancer Discovery 2014	GSE59810	Not applicable
Dataset 171	REC1_gsi-gsi_3	RNA-Seq	Stoeck et al., Cancer Discovery 2014	GSE59810	Not applicable
Dataset 172	REC1_gsi-wo_1	RNA-Seq	Stoeck et al., Cancer Discovery 2014	GSE59810	Not applicable
Dataset 173	REC1_gsi-wo_2	RNA-Seq	Stoeck et al., Cancer Discovery 2014	GSE59810	Not applicable
Dataset 174	REC1_gsi-wo_3	RNA-Seq	Stoeck et al., Cancer Discovery 2014	GSE59810	Not applicable

References

Bray, N.L., Pimentel, H., Melsted, P., and Pachter, L. (2016). Near-optimal probabilistic RNA-seq quantification. Nat Biotechnol *34*, 525-527.

Engreitz, J.M., Pandya-Jones, A., McDonel, P., Shishkin, A., Sirokman, K., Surka, C., Kadri, S., Xing, J., Goren, A., Lander, E.S.*, et al.* (2013). The Xist lncRNA exploits three-dimensional genome architecture to spread across the X chromosome. Science *341*, 1237973.

Fabbri, G., Holmes, A.B., Viganotti, M., Scuoppo, C., Belver, L., Herranz, D., Yan, X.J., Kieso, Y., Rossi, D., Gaidano, G.*, et al.* (2017). Common nonmutational NOTCH1 activation in chronic lymphocytic leukemia. Proceedings of the National Academy of Sciences of the United States of America *114*, E2911-E2919.

Gilbert, L.A., Horlbeck, M.A., Adamson, B., Villalta, J.E., Chen, Y., Whitehead, E.H., Guimaraes, C., Panning, B., Ploegh, H.L., Bassik, M.C.*, et al.* (2014). Genome-Scale CRISPR-Mediated Control of Gene Repression and Activation. Cell *159*, 647-661.

Klein, F.A., Pakozdi, T., Anders, S., Ghavi-Helm, Y., Furlong, E.E., and Huber, W. (2015). FourCSeq: analysis of 4C sequencing data. Bioinformatics *31*, 3085-3091.

Kluk, M.J., Ashworth, T., Wang, H., Knoechel, B., Mason, E.F., Morgan, E.A., Dorfman, D., Pinkus, G., Weigert, O., Hornick, J.L.*, et al.* (2013). Gauging NOTCH1 Activation in Cancer Using Immunohistochemistry. PLoS ONE *8*, e67306.

Landt, S.G., Marinov, G.K., Kundaje, A., Kheradpour, P., Pauli, F., Batzoglou, S., Bernstein, B.E., Bickel, P., Brown, J.B., Cayting, P.*, et al.* (2012). ChIP-seq guidelines and practices of the ENCODE and modENCODE consortia. Genome research *22*, 1813-1831.

Love, M.I., Huber, W., and Anders, S. (2014). Moderated estimation of fold change and dispersion for RNA-seq data with DESeq2. Genome Biology *15*.

Meerbrey, K.L., Hu, G., Kessler, J.D., Roarty, K., Li, M.Z., Fang, J.E., Herschkowitz, J.I., Burrows, A.E., Ciccia, A., Sun, T.*, et al.* (2011). The pINDUCER lentiviral toolkit for inducible RNA interference in vitro and in vivo. Proceedings of the National Academy of Sciences of the United States of America *108*, 3665-3670.

Ryan, R.J., Drier, Y., Whitton, H., Cotton, M.J., Kaur, J., Issner, R., Gillespie, S., Epstein, C.B., Nardi, V., Sohani, A.R.*, et al.* (2015). Detection of Enhancer-Associated Rearrangements Reveals Mechanisms of Oncogene Dysregulation in B-cell Lymphoma. Cancer discovery *5*, 1058-1071.

Shishkin, A.A., Giannoukos, G., Kucukural, A., Ciulla, D., Busby, M., Surka, C., Chen, J., Bhattacharyya, R.P., Rudy, R.F., Patel, M.M.*, et al.* (2015). Simultaneous generation of many RNA-seq libraries in a single reaction. Nat Methods *12*, 323-325.

Soneson, C., Love, M.I., and Robinson, M.D. (2015). Differential analyses for RNA-seq: transcript-level estimates improve gene-level inferences. F1000Res *4*, 1521.

Stoeck, A., Lejnine, S., Truong, A., Pan, L., Wang, H., Zang, C., Yuan, J., Ware, C., MacLean, J., Garrett-Engele, P.W.*, et al.* (2014). Discovery of biomarkers predictive of GSI response in triple-negative breast cancer and adenoid cystic carcinoma. Cancer discovery *4*, 1154-1167.

van de Werken, H.J., de Vree, P.J., Splinter, E., Holwerda, S.J., Klous, P., de Wit, E., and de Laat, W. (2012a). 4C technology: protocols and data analysis. Methods Enzymol *513*, 89-112.

van de Werken, H.J., Landan, G., Holwerda, S.J., Hoichman, M., Klous, P., Chachik, R., Splinter, E., Valdes-Quezada, C., Oz, Y., Bouwman, B.A.*, et al.* (2012b). Robust 4C-seq data analysis to screen for regulatory DNA interactions. Nat Methods *9*, 969-972.

Figure S1

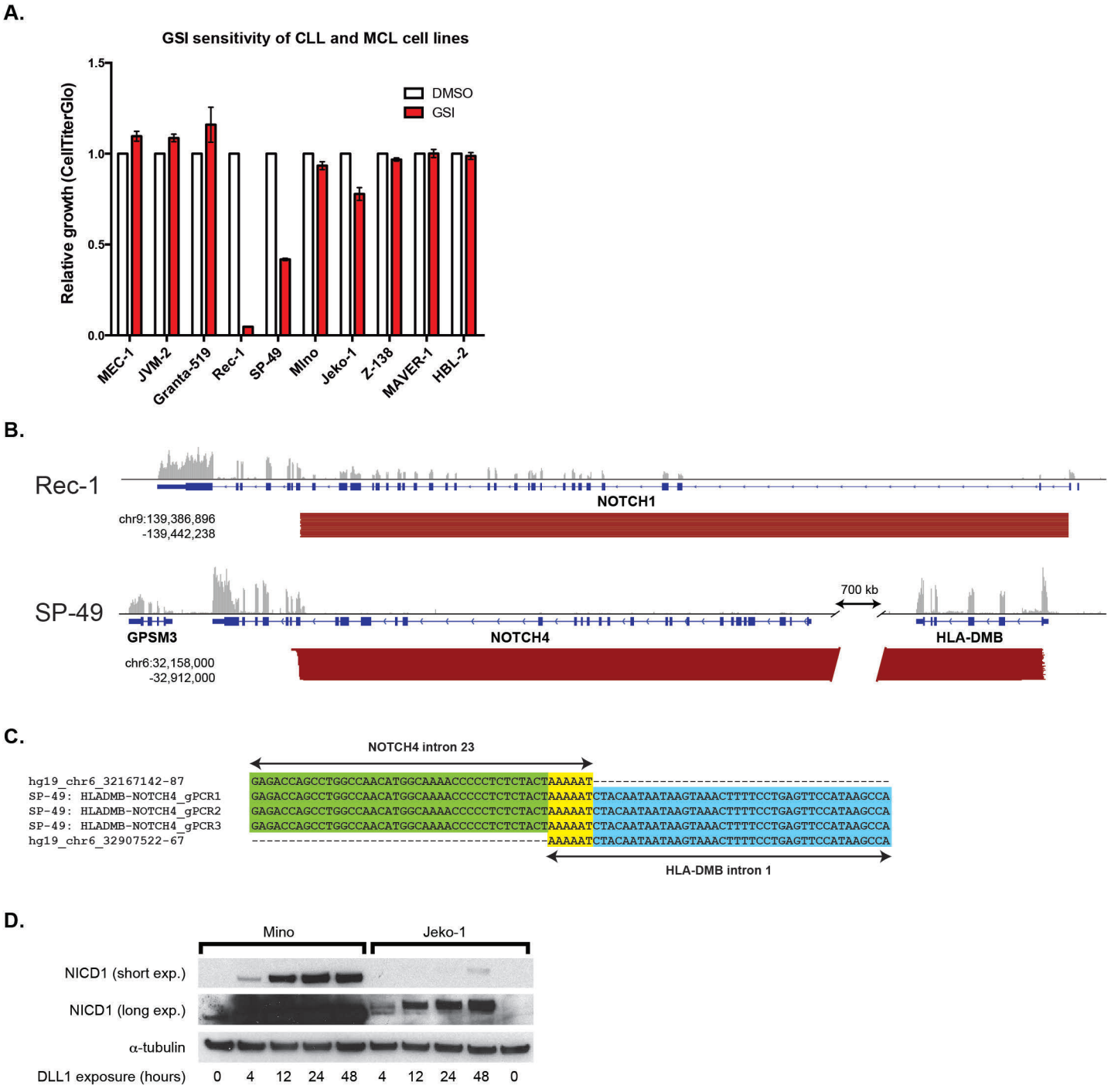

Figure S1. Notch signaling dependency and mechanisms of activation in MCL cell lines. Related to Figure 1. (**A**) Relative growth as measured by CellTiterGlo of MCL and CLL cell lines treated with GSI (compound E, 1μM) for 7 d. Data represent mean ± SEM (n=3). (**B**) RNA-Seq data showing aberrant Notch gene transcripts in MCL cell lines. Sequencing coverage is shown at top (gray). Red bars link read-pairs that demonstrate abnormal NOTCH1 transcript splicing (Rec-1, top), or a chimeric HLA-DMB and NOTCH4 transcript (SP-49, bottom); these abnormal transcripts are the result of interstitial genomic deletions involving chromosomes 9 and 6, respectively. (**C**) Alignment of Sanger sequencing results from SP-49 genomic DNA PCR with three independent primer pairs designed to amplify the HLA-DMB – NOTCH4 rearrangement junction. The junction contains a 6-bp region of micro-homology (yellow highlight) that is shared by the reference DNA sequences on both ends of the chromosome 6 deletion. (**D**) Western blot for NICD1 in Mino and Jeko cells plated on DLL1ext-IgG for the indicated time period.

Figure S2

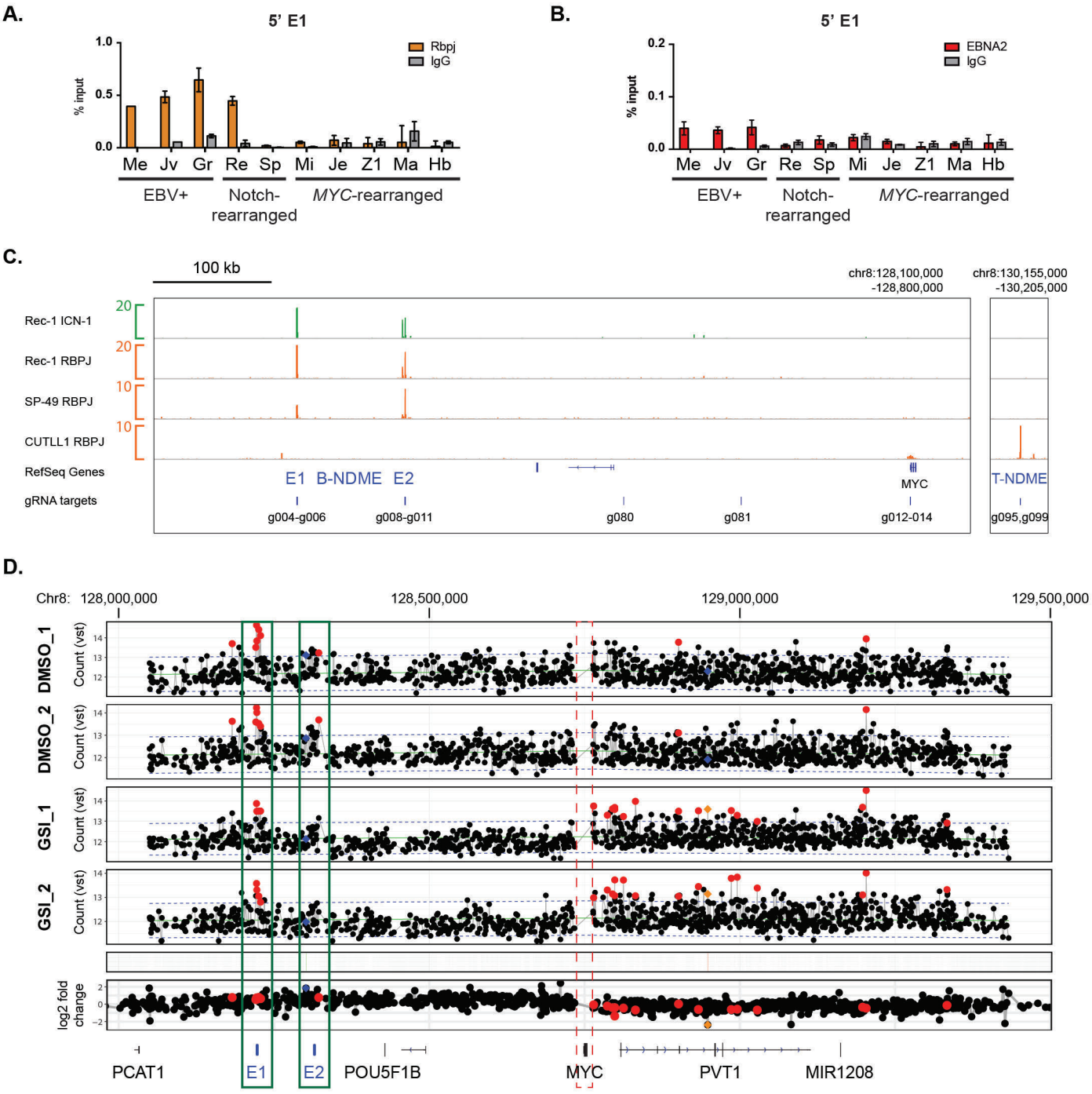

Figure S2. Notch and related transcription factor binding to 5' *MYC* enhancer sites. Related to Figure 2.
(A) ChIP-qPCR showing binding of RBPJ at 5' *MYC* enhancer E1 in CLL and MCL cell lines. Data represent mean ± SD. Note that while ChIP-PCR did not detect significant SP-49 RBPJ binding at E1, a significant peak was seen at E1 in RBPJ ChIP-Seq data, albeit weaker than binding seen in Rec-1 (see Figure 2G) **(B)** ChIP-qPCR showing binding of EBNA2 at 5' *MYC* enhancer E1 in CLL and MCL cell lines. Data represent mean ± SD. **(C)** Comparison of MCL cell line RBPJ ChIP-Seq binding at the *MYC* locus to published data from the T-ALL cell line CUTLL1. Position of sgRNAs targeting RBPJ-bound enhancers and other regions in the *MYC* locus are shown at bottom. **(D)** Replicate 4C-seq data from Rec-1 cells treated for 3 days with 1 μM Compound E (GSI) or DMSO, and processed with the FourCSeq pipeline (Klein et al., 2015). Each dot represents the normalized count for interactions between a given fragment and a viewpoint at the MYC promoter. For each condition, fragments showing contact intensity significantly greater than expected (z-score > 2, padj < 0.05) are colored red. Fragments showing significantly different contact intensity between the two treatments are colored blue. Orange dots mark fragments that satisfy both conditions for a given treatment. Signficantly interacting fragments are predominantly located within the 5' E1 and E2 enhancers in DMSO-treated replicates, while most significant interactions in GSI-treated cells are on the 3' side of MYC, including elements within the PVT1 gene body.

Figure S3

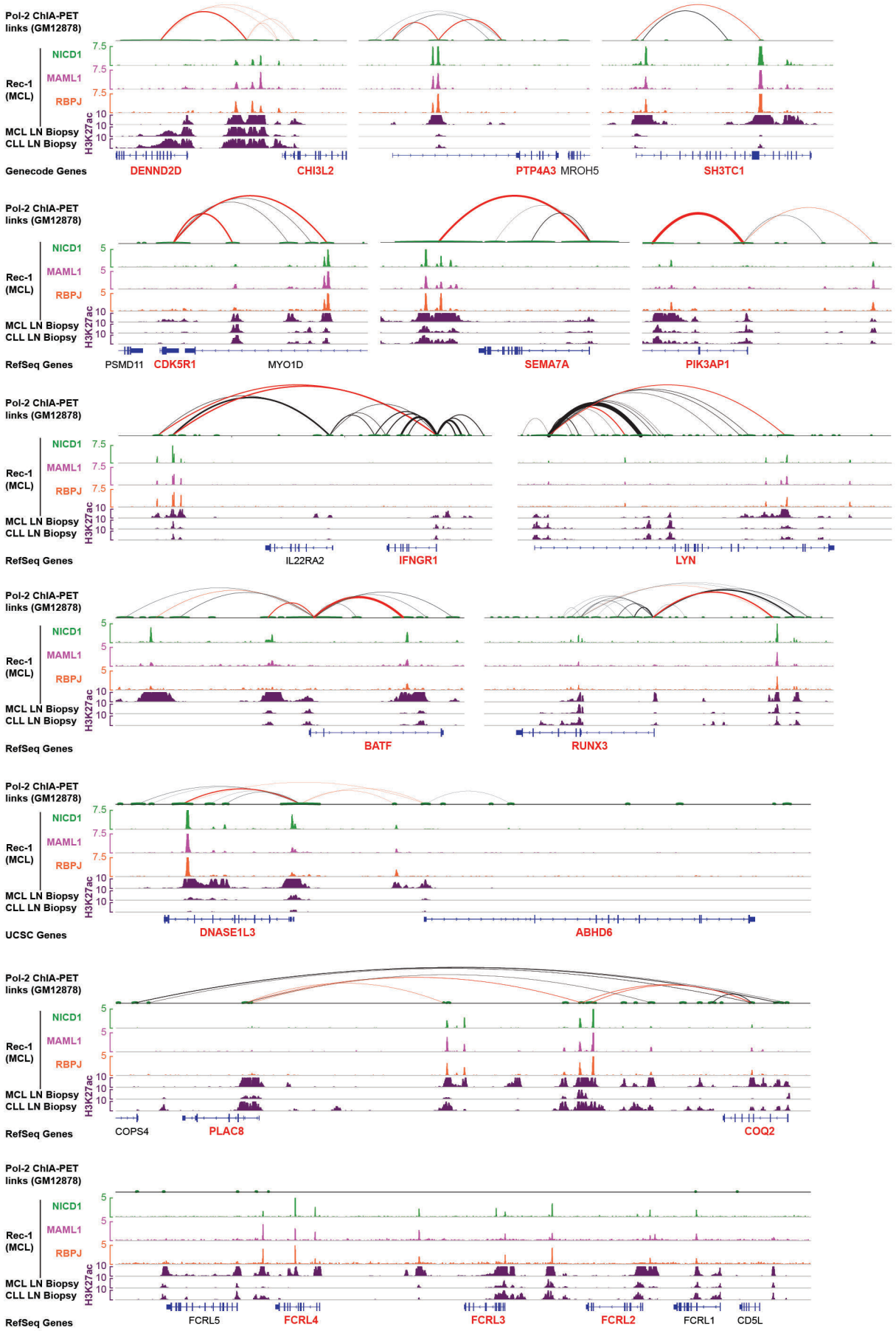

Figure S3. NTC protein binding and linkage to Notch-activated genes. Related to Figure 4.
Representative direct Notch target genes (red gene symbols) with GM12878 PolII ChIA-PET loops and NTC binding to distal enhancers and / or promoters, displayed as in Figure 4.

Figure S4.

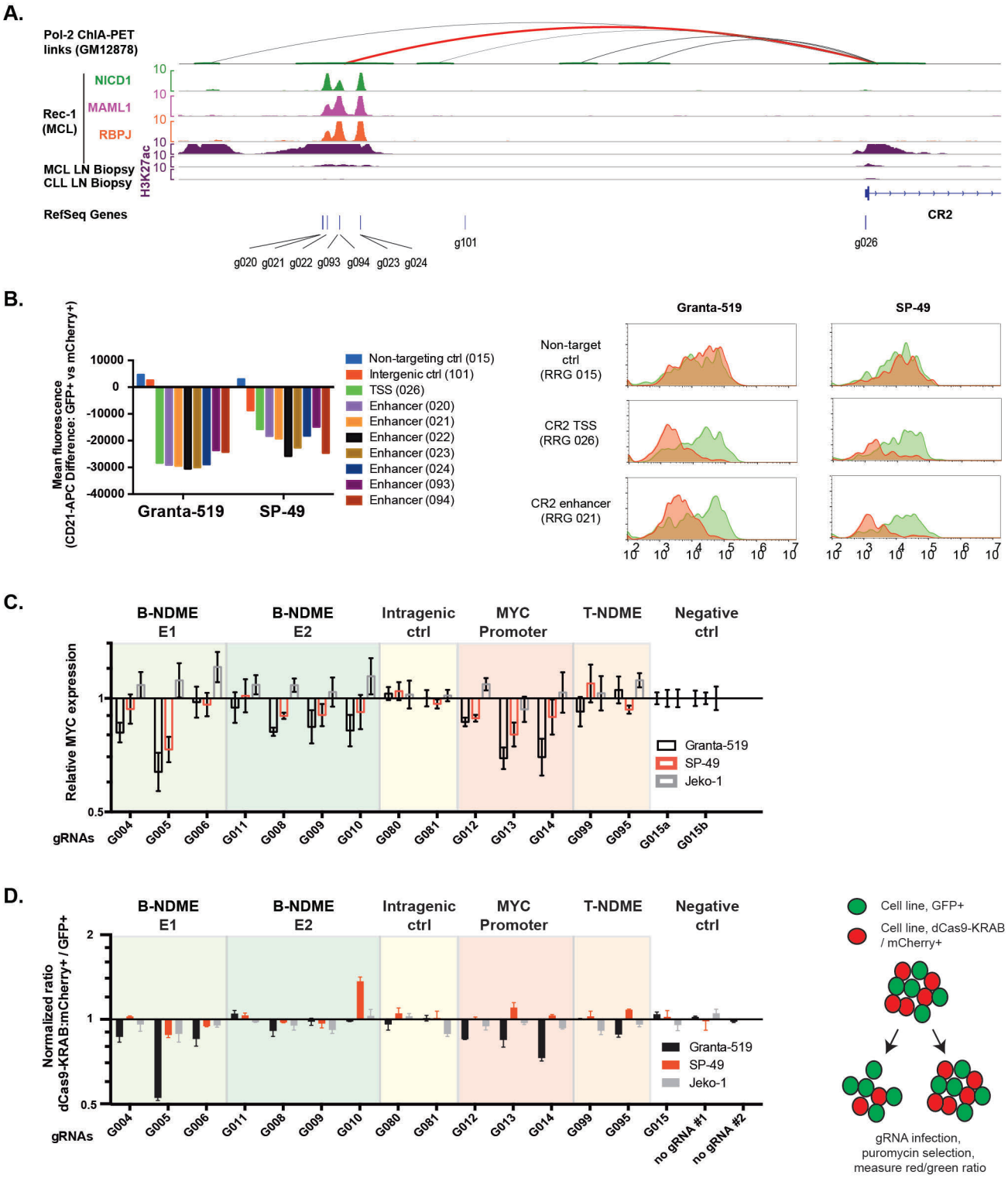

Figure S4. Effect of dCas9-KRAB repression of individual Notch target enhancers on gene expression and growth of MCL cell lines. Related to Figure 5.

(A) NTC-bound enhancers linked to the *CR2* gene (encoding CD21) and locations of sgRNA targeting. **(B)** Flow cytometric assessment of the effects of dCas9-KRAB targeting of NTC-bound enhancers on CD21 levels. A mixed population of KRAB-dCAS9-P2A-mCherry+ cells and GFP+ cells (derived from the indicated cell lines) were transduced with sgRNAs targeting the indicated regions in the *CR2* locus (or non-targeting control sgRNA). After selection, cells were harvested and stained with a CD21-APC antibody. Loss of CD21 was assessed by determining the difference in mean fluorescence between GFP+ and KRAB-dCAS9-P2A-mCherry+ cells. Representative flow histograms are shown at right, with data from mCherry+ cells shown as red curves, and data from GFP+ cells shown as green curves. **(C)** Effect of indicated sgRNAs on *MYC* expression (qRT-PCR) in KRAB-dCAS9-P2A-mCherry-expressing MCL cell lines. Expression was normalized to samples treated with a non-targeting sgRNA lentivirus. Data represent mean ± SD. **(D)** Left: Effect of sgRNAs on growth of MCL cell lines expressed as the ratio of KRAB-dCAS9-P2A-mCherry-expressing cells to GFP+ cells (no dCas9-KRAB repressor) after 7 d. Ratios were normalized to wells that did not contain sgRNA lentivirus or puromycin. Data represent mean ± SEM (n=2). Right: Schematic diagram of experimental strategy used to measure growth effects of *MYC* locus sgRNAs.

Figure S5

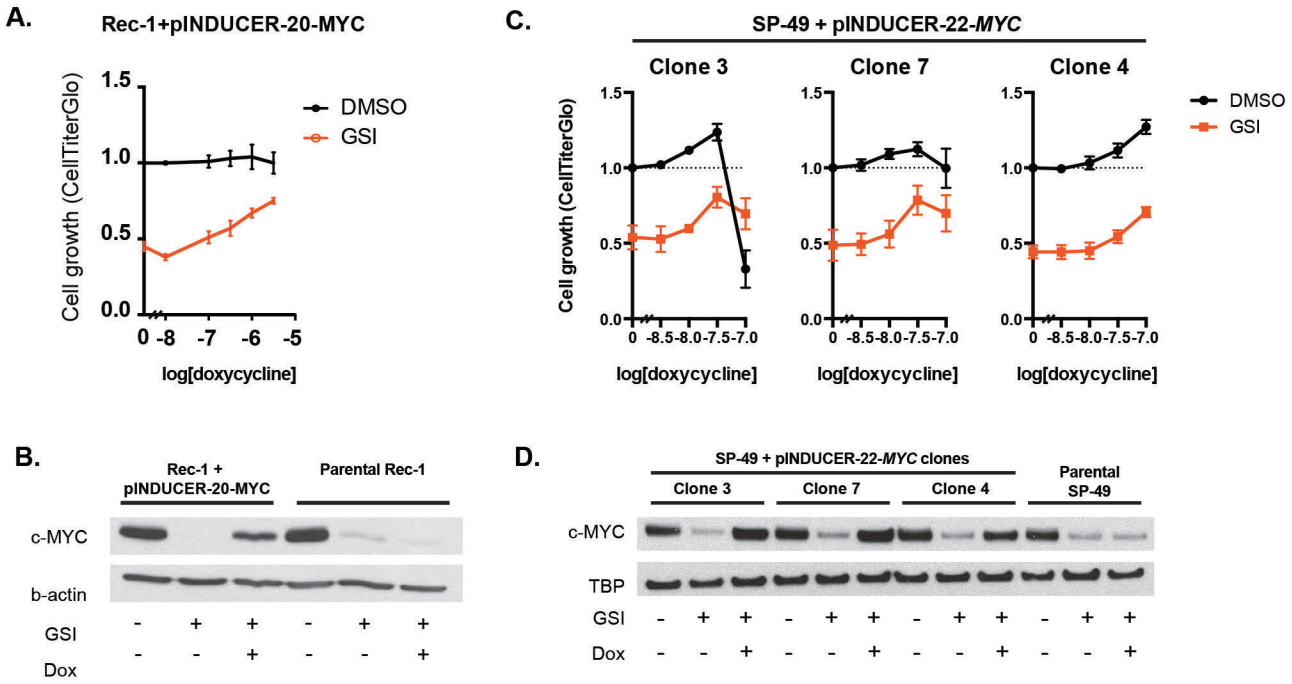

Figure S5. Dose-dependent rescue of GSI-sensitive MCL cell lines by *MYC* transgene induction. Related to Figure 5. **(A)** Doxycycline dose-response curves for rescue of cell growth in vehicle- or GSI-treated Rec-1 cells transduced with pINDUCER-20-MYC. GSI treatment was 1 μM Compound E for all experiments shown. Data represent mean ± SEM of 3 independent experiments. **(B)** Western blot showing rescue of MYC protein expression in G418-selected Rec-1 cells after transduction with pINDUCER-20-*MYC*. Cells were treated with vehicle, GSI, or GSI + 3.3 μg/ml doxycycline. **(C)** Doxycycline dose-response curves for rescue of cell growth in vehicle- or GSI-treated single-cell-derived SP-49 clones transduced with pINDUCER-22-*MYC*. Data represent mean ± SEM of 2 independent experiments. Note that two clones (3 and 7) show an optimal rescue dose lower than the maximum dose evaluated, with reduced cell growth / viability in both GSI-treated and untreated samples at higher doses. **(D)** Western blot showing *MYC* expression in single-cell-derived SP-49 clones transduced with pINDUCER-22-*MYC* and parental SP-49 treated with GSI or GSI + 100ng/ml doxycycline. Note that clones 3 and 7 show higher MYC expression in GSI + dox treated samples than in untreated samples at this dose, while clone 4 shows comparable MYC expression at baseline and in the presence of GSI + dox. Clone 4 showed optimal rescue at this dose, while clones 3 and 7 showed optimal rescue at a lower dose.

Figure S6

A.

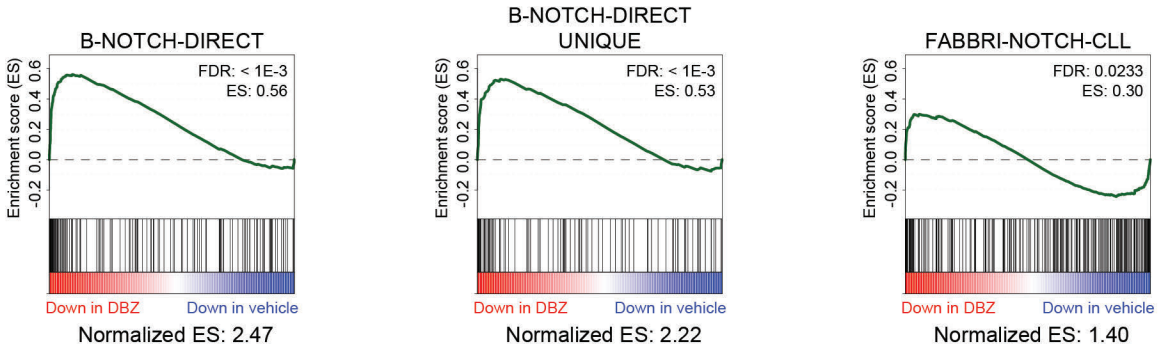

B.

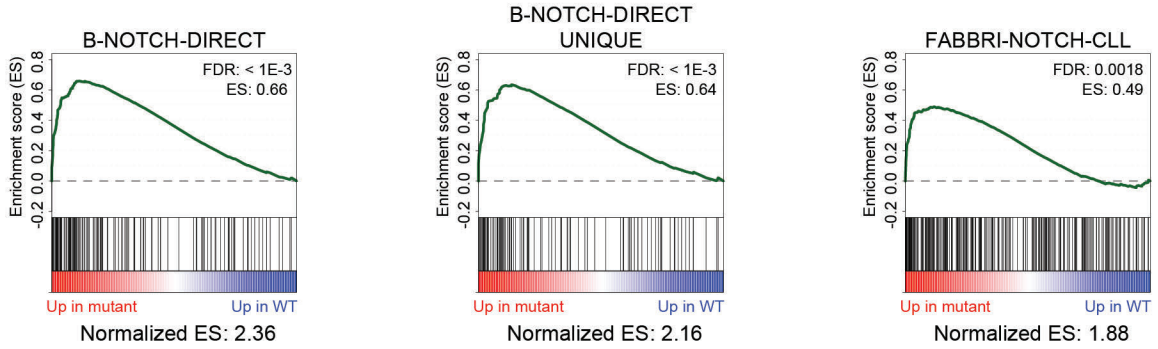

C.

CLL-M13 ChIP-Seq

		De novo motif analysis			Known motif analysis (RBPJ)	
Epitope	**Peaks**	**RBPJ logo**	**RBPJ rank**	**p-val**	**p-val**	**% of peaks**
NICD1	469		1	1e-68	1e-59	40.9%
RBPJ	14,466		4	1e-287	1e-178	20.3%

Figure S6. Analysis of Notch target gene expression and NTC binding in MCL xenografts and CLL lymph node biopsies. Related to Figures 6 and 7.

(A) GSEA of MCL PDX 98848 RNA-seq data, comparing enrichment for the direct Notch target signature (B-NOTCH-DIRECT, as shown in Figure 6C) to enrichment for the NICD1-activated gene signature identified in a CLL cell line (FABBRI-NOTCH-CLL, Fabbri et al., 2017), and the set of genes unique to the former, but not the latter signature (B-NOTCH-DIRECT_UNIQUE). FDR = FDR-adjusted p-value. ES = enrichment score. Genes were ranked according to fold-change in vehicle versus DBZ-treated mice. **(B)** GSEA of CLL biopsy RNA-Seq data, comparing enrichment for the direct Notch target gene set defined in MCL cell line experiments (B-NOTCH-DIRECT, as shown in Figure 7C) to the gene set defined in Fabbri et al., 2017 and the set of genes unique to MCL experiments as described above. Genes were ranked according to fold-change in NOTCH1 mutant versus NOTCH1 wild-type CLL lymph node biopsies. **(C)** Summary of peak calling and motif analysis on NICD1 and RBPJ ChIP-Seq datasets generated from lymph node biopsy tissue diffusely involved by CLL-M13 (*NOTCH1* mutant). 'Peaks' denotes the number of significant genome-wide peaks detected by Homer findPeaks using the 'factor' style (default FDR < 0.001). For each dataset, the logo, rank, and p-value are shown for the motif detected in de novo HOMER findMotifs analysis that most closely matched the known RBPJ motif from the HOMER library. Statistics shown for analysis with the pre-defined RBPJ motif (HOMER known motif library) include enrichment p-value and percentage of peaks with at least one above-threshold match to the known RBPJ motif.

Figure S7

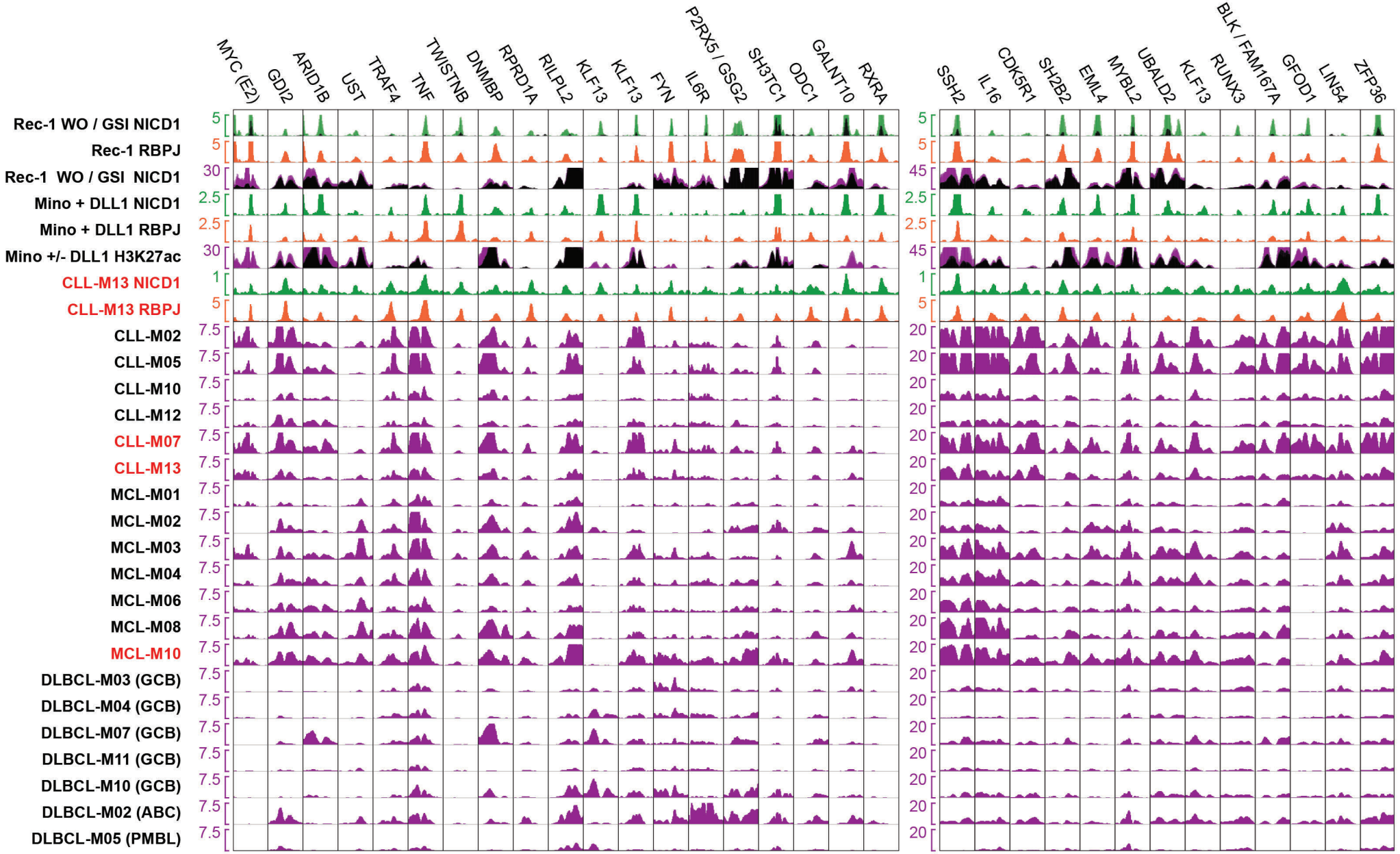

Figure S7. Notch transcription factor binding and histone acetylation at Notch regulatory elements in MCL cell lines and lymphoma patient biopsies. Related to Figure 7.
Each column displays a 2.2 kB genomic window centered on an NTC binding site that showed significant NICD1 and RBPJ binding in the CLL patient lymph node biopsy CLL-M13. Each element also showed NTC factor binding and linkage to a direct Notch target gene in MCL cell line analysis. Linked target genes are listed at top (some elements are linked to more than one gene, and KLF13 is linked to three elements). The bottom 20 tracks show H3K27ac ChIP-Seq signal for six CLL lymph node biopsies, seven MCL biopsies, and seven biopsies from diffuse large B cell lymphoma (DLBCL) variants (five germinal center B cell-like DLBCL, GCB, one activated B cell-like DLBCL, ABC, and one primary mediastinal large B cell lymphoma, PMBL, as indicated). CLL and MCL biopsies bearing PEST domain truncating mutations in *NOTCH1* are indicated in red, while all other CLL and MCL biopsies are *NOTCH1* wild-type. Note that most, but not all Notch regulatory elements show greater acetylation in CLL and MCL compared to DLBCL. The six tracks at top show TF binding and histone acetylation in MCL cell lines. NICD1 and H3K27ac tracks in Rec1 show signal in both the Notch-on state (GSI washout, colored track) and Notch-off state (mock-washout, black overlay). Mino H3K27ac tracks show signal following 48 hours of DLL1-IgG stimulation (colored track) or control-ligand stimulation (black overlay).